Research Article

Wasim Jamshed, Ramanahalli Jayadevamurthy Punith Gowda, Rangaswamy Naveen Kumar, Ballajja Chandrappa Prasannakumara, Kottakkaran Sooppy Nisar*, Omar Mahmoud, Aysha Rehman, and Amjad Ali Pasha

Entropy production simulation of second-grade magnetic nanomaterials flowing across an expanding surface with viscidness dissipative flux

https://doi.org/10.1515/ntrev-2022-0463
received February 23, 2022; accepted July 10, 2022

Abstract: The principal focal point of the current review is the second-grade nanofluid (SGNF) stream with slanted magnetohydrodynamics and viscous disintegration impacts across a moving level flat surface with entropy investigation. Here, we have done a comparative study on copper–methanol and iron–methanol second-grade nanoliquids. The governing conditions of the SGNF model are changed into ordinary differential equations (ODEs) by using supportive changes. To tackle the non-straight ODEs, the Runge-Kutta Fehlberg-45 procedure is utilized. The result reveals that the velocity gradient of copper–methanol second-grade nanoliquid is strongly affected by suction, magnetic, and second-grade fluid parameters and declines faster when compared to iron–methanol second-grade nanoliquid. Copper–methanol SGNF shows improved heat transfer than iron–methanol SGNF for improved values of Eckert and Biot numbers.

Keywords: second-grade nanofluid, inclined magnetic effect, Joule heating, entropy generation

*** Corresponding author: Kottakkaran Sooppy Nisar,** Department of Mathematics, Prince Sattam Bin Abdulaziz University, Wadi Aldawaser, 11991, Saudi Arabia, e-mail: n.sooppy@psau.edu.sa
Wasim Jamshed: Department of Mathematics, Capital University of Science and Technology (CUST), 44000, Islamabad, Pakistan
Ramanahalli Jayadevamurthy Punith Gowda, Rangaswamy Naveen Kumar, Ballajja Chandrappa Prasannakumara: Department of Studies and Research in Mathematics, Davangere University, Davangere 577002, Karnataka, India
Omar Mahmoud: Petroleum Engineering Department, Faculty of Engineering and Technology, Future University in Egypt, New Cairo 11835, Egypt
Aysha Rehman: Department of Mathematics, University of Gujrat, Gujrat 50700, Pakistan
Amjad Ali Pasha: Aerospace Engineering Department, King Abdulaziz University, Jeddah 21589, Saudi Arabia

Nomenclature

A	unsteadiness parameter
$A_{ç1}$, $A_{ç2}$	Rivlin–Ericksen tensors
$\mathrm{Bi}_ç$	Biot number
Br	Brinkman number
C_f	skin friction
d/dt	material time derivative
Ec	Eckert number
$f(\eta)$	non-dimensional velocity profiles
h_f	coefficient of heat transfer rate
I	identity tensor
k	thermal conductivity
k_0	thermal conductivity of solid
k^*	mean absorption coefficient
K	porous medium parameter
M	magnetic parameter
N_r	radiation parameter
Nu_x	Nusselt number
p	pressure
Pr	Prandtl number
q_r	radiative heat flux
Re_f	local Reynolds number
S	mass transfer variable
T	temperature
T_∞	ambient temperature
(u, v)	velocity components
V	fluid velocity
V_w	porous stretching surface
(x, y)	directions
α	second-grade parameter

α_f	thermal diffusivity parameter
α_1 and α_2	material variables
Γ	angle of inclination
η	dimensionless similarity coordinate
$\theta(\eta)$	dimensionless thermal profile
μ	dynamic viscosity
ν	kinematic viscosity
ρ	density
ρC_p	heat capacitance
σ	electrical conductivity
σ^*	Stefan–Boltzmann constant
Ω	dimensionless thermal gradient
Λ	velocity slip variable
ϕ	volumetric fraction coefficient

Subscripts

f	fluid
nf	nanofluid
s	solid nanoparticle
w	wall/surface
∞	ambient

1 Introduction

A few fluid dynamics problems have appreciated the attention given to the flow involving non-Newtonian liquids because of their application in industry and technology. It is well known that engineers, physicists, and mathematicians face a superior challenge in the dynamics of non-Newtonian fluids. In many fields, including food, drilling operations, and bio-engineering, non-linearity can manifest itself in a number of ways. For such fluids, the Navier–Stokes principle is insufficient and no single constitutive equation is available in the literature that exhibits the properties of all fluids. Many fluid models have been proposed as a consequence of the complex behavior of such fluids. Among these, viscoelastic-type liquids have received much attention. The subclass of viscoelastic liquids is the second-grade liquid (SGL) model that can reasonably be expected to have an analytical solution. Nowadays, major research is being carried out on the regime of non-Newtonian liquids due to their considerable functional efficiency. Sahoo *et al.* [1] quizzed the aspects of Joule heating and slip impact on the magnetohydrodynamic (MHD) stream of SGL past a sheet with viscous dissipation. Imtiaz *et al.* [2] pondered the Ohmic and magnetic effects to deliberate SGL flow provoked by the rotating disk. Hayat *et al.* [3] quizzed the SGL stream with nanoparticle suspension over a sheet with magnetic impact. Kalaivanan *et al.* [4] deliberated the activation energy effect on the SGL stream on a surface with stretching. Wakeel Ahmed *et al.* [5] quizzed the upshot of modified-Fourier heat flux on SGL with nanoparticle suspension past a stretchy geometry.

In recent years, the modeling and analysis of nanofluid flows have become a frequent area of study. Nanofluids are being developed as a breakthrough means of improving heat transmission. Nanoparticles may be used to overcome cooling issues in thermal frameworks by using heat transport fluids containing suspended nanoparticles. In connection with this, numerous investigators examined the stream of nanoliquids over dissimilar surfaces. Shafiq *et al.* [6] swotted the bioconvection steam of SGL with nanoparticle suspension past a surface with a chemical reaction effect. Gowda *et al.* [7] swotted the thermophoresis effect on liquid flow with twin nanoparticle suspensions past a poignant disk. Christopher *et al.* [8] scrutinized the chemical reaction power of hybrid nanoliquid flow on a cylinder. Jayadevamurthy *et al.* [9] examined a bioconvection stream of fluid with dual nanoparticle suspension on a poignant disk with spin. Hayat *et al.* [10] quizzed the magnetic field upshot on the SGL stream past the Riga wall.

Nuclear engineering relies heavily on the magnetic effect and Ohmic heating. In Joule or Ohmic heating, electricity flows into an item and creates heat at the same time. A number of scholars have explored the boundary layer stream issues with Joule heating on various geometric forms. Shashikumar *et al.* [11] studied the Brinkman–Forchheimer stream in a microchannel with numerous slips, viscous dissipation, and Ohmic heating. According to Hayat *et al.* [12], Ohmic heating and melting may have a major influence on the flow of viscous fluid over a stretchable plate. Dusty hybrid nanoliquid flow was studied by Radhika *et al.* [13] for the stimulation of the magnetic effect. The stream of a Sisko nanoliquid owing to a spinning disk was examined by Ijaz *et al.* [14] with radiation effects. The MHD flow of hybrid nanoliquids through an disk with activation energy was examined by Reddy *et al.* [15].

The effects of viscous dissipation are often ignored, but when the liquid viscosity is high, its presence becomes important. It alters the distribution of temperatures by playing a role as a source of energy that affects the rates of heat transfer. Hayat *et al.* [16] debriefed the viscous dissipation upshots in the nanoliquid stream initiated by a disk. Sithole *et al.* [17] quizzed the radiation effect on the MHD flow of SGL with suspended nanoparticles past a sheet. Hazarika *et al.* [18] reduced the solutions

for the MHD stream of nanofluid past a sheet with viscous dissipation. The upshot of Joule heating in the radiative heat transport of non-Newtonian liquids like power-law, third-grade, and Jeffery fluids is an essential factor for scientists because of their dynamic applications in micro-fluidic devices, micro-electromechanical systems, aerospace, and chemical reactors. Enthused by these applications, several scholars scrutinized the stimulation of Joule heating and thermal radiation on diverse liquid streams. Gireesha *et al.* [19] deliberated the impact of radiation on the MHD flow of Jeffrey nanoliquid past a porous extending sheet. Shit and Mandal [20] quizzed the entropy creation on MHD flow of Casson nanoliquid on an extending surface with radiation effect.

During the past several decades, several researchers concentrating on the generation of entropy have conducted various studies on energy production in diverse fluid stream conditions. Thermodynamic performance is a thought-provoking characteristic of building the right apparatus when energy saving is a foremost issue. The relevance of entropy generation in liquid flow, as well as its importance in several industrial applications such as ACs, heat pumps, and fire engines, has encouraged many researchers. Bejan [21] was the first to bring up the topic of entropy management. He demonstrated that thermofluidic systems can be treated with characteristics of entropy and provided a calculation formulation for the production rate of entropy. Captivated by these indications, many researchers discuss the generation of entropy in several fluid streams through different surfaces. Yusuf *et al.* [22] quizzed the generation of entropy in an MHD Williamson nanoliquid stream passing over a sheet. Azam *et al.* [23] looked at the production of entropy in a Williamson fluid flow with nanoparticle suspensions while accounting for Ohmic heating. Bhatti *et al.* [24] quizzed the formation of entropy in a Williamson liquid stream with nanoparticle suspension while accounting for thermophoretic and Brownian motion. Alsaadi *et al.* [25] quizzed the paraphernalia of radiative heat flux on the MHD stream of Williamson nanomaterial liquid on a surface. Refs. [26–40] include new additions that consider conventional and nanofluids with heat and mass transmission in various physical circumstances.

The aforementioned writing features the basic elements of the liquid stream across different calculations. The progression of SGL fluid over a moving surface with a thermal radiation impact has not yet been explored. As a result, the primary goal of this study is to investigate the features of non-uniform stretching velocity with thermal radiation, Ohmic, and viscous dissipation effects in an SGL stream. In addition, graphical representations are used to explain the main effects of various non-dimensionless factors on fluid profiles.

2 Mathematical formulation

The mathematical representation of the moving flat horizontal surface with non-uniform stretching velocity is given as follows:

$$U_w(x, t) = \frac{bx}{1 - \xi t}, \tag{2.1}$$

where b is the initial rate of stretching of the porous sheet. $T_w(x, t) = T_\infty + \frac{b^\star x}{1-\xi t}$ is the temperature of the insulated sheet under consideration, and for the sake of ease, the sheet's left end is supposed to be fixed at $x = 0$. Furthermore, the temperature variation rate is represented by $b^\star$. The mathematical model is considered under the following conditions and assumptions (Figure 1):

- Second-grade nanofluid (SGNF)
- Tiwari and Das nanofluid model
- Porous medium
- Porous stretching flat surface
- Laminar unsteady flow
- Viscous dissipation
- Radiative heat flux
- Newton and slip boundary conditions.

The Cauchy stress tensor in an SGL is mathematically represented as follows (see, for details, Shah *et al.* [41]):

$$S^\star = \mu A_{\varsigma 1} + \alpha_1 A_{\varsigma 2} + \alpha_1 A_{\varsigma 1}^2 - pI, \tag{2.2}$$

$$A_{\varsigma 1} = (\text{grad V}) + (\text{grad V})^T, \tag{2.3}$$

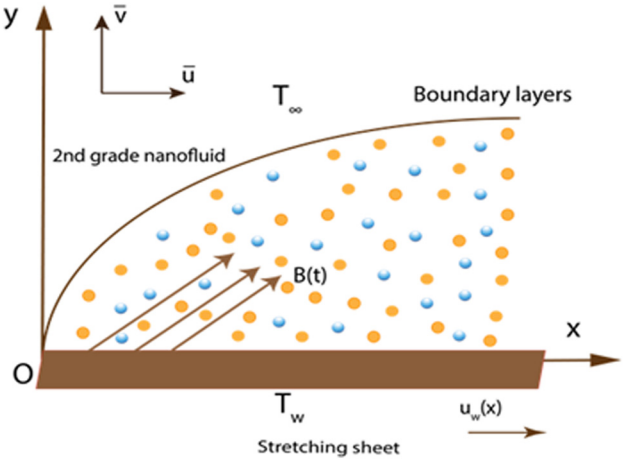

Figure 1: Flow geometry.

$$A_{\varsigma 2} = \frac{\mathrm{d}A_{\varsigma 1}}{\mathrm{dt}} + A_{\varsigma 1}(\mathrm{grad\ V}) + A_{\varsigma 1}(\mathrm{grad\ V})^{T}. \quad (2.4)$$

The Clausius–Duhem inequality is confirmed. Furthermore, we find that the Helmholtz free energy is minimal in equilibrium for the liquid is at rest when

$$\mu \geq 0,\ \alpha_1 \geq 0,\ \alpha_1 + \alpha_2 = 0. \quad (2.5)$$

If $\alpha_1 + \alpha_2 = 0$, then the equation of SGL reduces to a viscous liquid.

The SGNF flow equations [41] under normal boundary layer assumptions, viscous dissipation, and joule heating with radiation heat flux are as follows:

$$\frac{\partial u}{\partial x} + \frac{\partial v}{\partial y} = 0, \quad (2.6)$$

$$\begin{aligned}&\frac{\partial u}{\partial t} + u\frac{\partial u}{\partial x} + v\frac{\partial u}{\partial y}\\ &= \frac{\alpha_1}{\rho_{nf}}\left[\frac{\partial u}{\partial x}\left(\frac{\partial^2 u}{\partial y^2}\right) + \left(\frac{\partial^3 u}{\partial t \partial y^2}\right) + u\left(\frac{\partial^3 u}{\partial x \partial y^2}\right)\right.\\ &\quad \left. + \frac{\partial u}{\partial y}\left(\frac{\partial^2 v}{\partial y^2}\right) + v\left(\frac{\partial^3 u}{\partial y^3}\right)\right]\\ &\quad + \frac{\mu_{nf}}{\rho_{nf}}\left(\frac{\partial^2 u}{\partial y^2}\right) - \frac{\sigma_{nf}B^2(t)}{\rho_{nf}}u\sin^2(\Gamma),\end{aligned} \quad (2.7)$$

$$\begin{aligned}&\frac{\partial T}{\partial t} + u\frac{\partial T}{\partial x} + v\frac{\partial T}{\partial y}\\ &= \frac{k_{nf}}{(\rho C_p)_{nf}}\left(\frac{\partial^2 T}{\partial y^2}\right) - \frac{1}{(\rho C_p)_{nf}}\left(\frac{\partial q_r}{\partial y}\right)\\ &\quad + \frac{\mu_{nf}}{(\rho C_p)_{nf}}\left(\frac{\partial u}{\partial y}\right)^2 + \frac{\sigma_{nf}}{(\rho C_p)_{nf}}B^2(t)u^2\sin^2(\Gamma).\end{aligned} \quad (2.8)$$

The relevant boundary conditions are as follows:

$$\begin{aligned}&u(x, 0) = U_w + N_w\left(\frac{\partial u}{\partial y}\right),\\ &v(x, 0) = V_w,\ -k_0\left(\frac{\partial T}{\partial y}\right) = h_f(T_w - T),\end{aligned} \quad (2.9)$$

$$u \to 0,\ \frac{\partial u}{\partial y} \to 0,\ T \to T_\infty \ \text{as}\ y \to \infty. \quad (2.10)$$

The dispersion of nanoparticles into methanol liquid causes improved thermophysical features. Table 1 summarizes the material parameters for the SGNF (see, for example, refs. [42–46]).

Table 1: Thermophysical features of second-grade nanoliquid

Properties	Nanofluids
Dynamics viscosity	$\mu_{nf} = \mu_f(1-\phi)^{-2.5}$
Density	$\rho_{nf} = (1-\phi)\rho_f + \phi\rho_s$
Heat capacity	$(\rho C_p)_{nf} = (1-\phi)(\rho C_p)_f + \phi(\rho C_p)_s$
Thermal conductivity	$\frac{k_{nf}}{k_f} = \left[\frac{(k_s+2k_f)-2\phi(k_f-k_s)}{(k_s+2k_f)+\phi(k_f-k_s)}\right]$
Electrical conductivity	$\frac{\sigma_{nf}}{\sigma_f} = \left[1 + \frac{3\left(\frac{\sigma_s}{\sigma_f}-1\right)\phi}{\left(\frac{\sigma_s}{\sigma_f}+2\right)-\left(\frac{\sigma_s}{\sigma_f}-1\right)\phi}\right]$

The material features of the methanol and the nanoparticles being utilized in this work are given in Table 2 (see, for instance, refs. [47–49]).

Using the Roseland approximation, Brewster [50], one can write

$$q_r = -\frac{4\sigma^*}{3k^*}\frac{\partial ¥^4}{\partial y}. \quad (2.11)$$

3 Solution to the problem

By using the similarity approach to the governing partial differential equations, equations (2.1)–(2.3) of boundary value problems have been transformed into ordinary differential equations (ODEs). The stream function can be defined as

$$u = \frac{\partial \psi}{\partial y},\ v = -\frac{\partial \psi}{\partial x}, \quad (3.1)$$

and similarity variables of the form

$$\begin{aligned}&\chi(x, y) = \sqrt{\frac{b}{\nu_f(1-\xi t)}}\,y,\\ &\psi(x, y) = \sqrt{\frac{\nu_f b}{(1-\xi t)}}\,xf(\chi),\ \theta(\chi) = \frac{T - T_\infty}{T_w - T_\infty},\end{aligned} \quad (3.2)$$

into equations (2.1)–(2.3). We obtain

Table 2: Primary properties of the base fluid and nanoparticles at a standard temperature

Thermophysical properties	ρ (kg/m^3)	C_p (J/kg K)	k (W/m K)	σ (S/m)
Copper (Cu)	8,933	385	401	5.96×10^7
Iron (Fe_3O_4)	5,180	670	9.7	0.74×10^6
Methanol (MeOH)	792	2,545	0.2035	0.5×10^{-6}

$$f''' + \phi_1 \left[\begin{array}{l} \phi_2 \left(ff'' - f'^2 - A\left(\frac{\chi}{2} f'' + f' \right) \right) + \alpha (2f'f''' \\ + A\left(2f'' + \frac{\chi}{2} f^{iv} \right) - f''^2 - ff^{iv}) \\ - \frac{\phi_4}{\phi_2} M \sin^2(\Gamma) f' \end{array} \right] = 0, \tag{3.3}$$

$$\theta'' \left(1 + \frac{1}{\phi_4} \mathrm{Pr} N_r \right) + \mathrm{Pr} \frac{\phi_3}{\phi_5} \left[f\theta' - f'\theta - A\left(\theta + \frac{\chi}{2} \theta' \right) + \frac{\mathrm{Ec}}{\phi_1 \phi_3} f''^2 + \frac{\phi_4}{\phi_3} M \mathrm{Ec} \sin^2(\Gamma) f'^2 \right] = 0, \tag{3.4}$$

with

$$\left. \begin{array}{l} f(0) = S,\ f'(0) = 1 + \Lambda f''(0), \\ \theta'(0) = -\mathrm{Bi}_{\varsigma}(1 - \theta(0)) \\ f'(\chi) \to 0, f''(\chi) \to 0,\ \theta(\chi) \to 0,\ \text{as} \chi \to \infty \end{array} \right\}, \tag{3.5}$$

where $\phi_i's$ is $1 \le i \le 5$ in equations (3.3) and (3.4) representing the following thermophysical properties for the SGNF:

$$\left. \begin{array}{l} \phi_1 = (1 - \phi)^{2.5},\ \phi_2 = \left(1 - \phi + \phi \frac{\rho_s}{\rho_f} \right), \\ \phi_3 = \left(1 - \phi + \phi \frac{(\rho C_p)_s}{(\rho C_p)_f} \right), \\ \phi_4 = \left(1 + \frac{3\left(\frac{\sigma_s}{\sigma_f} - 1 \right)\phi}{\left(\frac{\sigma_s}{\sigma_f} + 2 \right) - \left(\frac{\sigma_s}{\sigma_f} - 1 \right)\phi} \right), \\ \phi_5 = \left(\frac{(k_s + 2k_f) - 2\phi(k_f - k_s)}{(k_s + 2k_f) + \phi(k_f - k_s)} \right). \end{array} \right\} \tag{3.6}$$

Equation (2.1) is satisfied identically. In the above equations, $'$ takes derivatives w.r.t χ, where $A = \frac{\xi}{\mathrm{b}}$, $\alpha = \frac{\alpha_1 b}{\mu_f}$ and $K = \frac{\nu_f(1-\xi t)}{bk}$, $\mathrm{Pr} = \frac{\nu_f}{\alpha_f}$, $N_r = \frac{16}{3} \frac{\sigma^* ¥_{\infty}^3}{\kappa^* \nu_f (\rho C_p)_f}$, $\alpha_f = \frac{\kappa_f}{(\rho C_p)_f}$, $S = -V_w \sqrt{\frac{1-\xi t}{\nu_f b}}$. $\Lambda = \sqrt{\frac{b}{\nu_f(1-\xi t)}} \mu_f$, $\mathrm{Ec} = \frac{U_w^2}{(C_p)_f (T_w - T_{\infty})}$, and $\mathrm{Bi}_{\varsigma} = \frac{h_f}{k_0} \sqrt{\frac{\nu_f(1-\xi t)}{b}}$.

The skin friction (C_f) and the local Nusselt number (Nu_x) can be stated as follows (see, for example, Shah *et al.* [41]):

$$C_f = \frac{\tau_w}{\rho_f U_w^2}, \mathrm{Nu}_x = \frac{x q_w}{k_f (T_w - T_{\infty})}, \tag{3.7}$$

where τ_w and q_w represent the heat flux determined by

$$\left. \begin{array}{l} \tau_w = \left(\mu_{nf} \frac{\partial u}{\partial y} + \alpha_1 \left(\frac{\partial^2 u}{\partial t \partial y} + u \frac{\partial^2 u}{\partial x \partial y} + 2 \frac{\partial u}{\partial y} \frac{\partial u}{\partial x} + \nu \frac{\partial^2 u}{\partial^2 y} \right) \right)_{y=0}, \\ q_w = -k_{nf} \left(1 + \frac{16}{3} \frac{\sigma^* T_{\infty}^3}{\kappa^* \nu_f (\rho C_p)_f} \right) \left(\frac{\partial T}{\partial y} \right)_{y=0}. \end{array} \right\} \tag{3.8}$$

Applying the non-dimensional transformations (3.2), one obtains

$$\left. \begin{array}{l} C_f \mathrm{Re}_x^{\frac{1}{2}} = \left(\frac{f''(0)}{(1-\phi)^{2.5}} + \alpha \left(3f''(0)f'(0) - f'''(0)f(0) \right. \right. \\ \left. \left. + \frac{A}{2} (\chi f'''(0) + 3f''(0)) \right) \right), \\ \mathrm{Nu}_x \mathrm{Re}_x^{-\frac{1}{2}} = -\frac{k_{nf}}{k_f} (1 + N_r) \theta'(0). \end{array} \right\} \tag{3.9}$$

4 Entropy generation minimization

There is a constant fear among scientists and engineers that valuable energy will be squandered. A thorough entropy generation study of the system causing irreversible useful energy is thus essential. MHD is a non-ideal phenomenon that results in a growth in the system's entropy. Then, we have [51]

$$E_G = \frac{k_{nf}}{T_{\infty}^2} \left\{ \left(\frac{\partial T}{\partial y} \right)^2 + \frac{16}{3} \frac{\sigma^* T_{\infty}^3}{\kappa^* \nu_f (\rho C_p)_f} \left(\frac{\partial T}{\partial y} \right)^2 \right\} + \frac{\mu_{nf}}{T_{\infty}} \left(\frac{\partial u}{\partial y} \right)^2 + \frac{\sigma_{nf} B^2(t) \sin^2(\Gamma) u^2}{T_{\infty}}. \tag{4.1}$$

This equation's first component reflects the irreversibility of heat transmission, the second term is related to fluid friction, and the third is related to inclined MHD phenomena.

NG represents the dimensionless entropy generation, which is defined as [52–56]:

$$\mathrm{NG} = \frac{T_{\infty}{}^2 b^2 E_G}{k_f (T_w - T_{\infty})^2}. \tag{4.2}$$

According to equation (3.2), the non-dimensional form of the entropy equation can be determined as follows:

$$\mathrm{NG} = \mathrm{Re} \left(\phi_5 (1 + N_r) \theta'^2 + \frac{1}{\phi_1} \frac{\mathrm{Br}}{\Omega} (f''^2 + \phi_1 \phi_4 M \sin^2(\Gamma) f'^2) \right). \tag{4.3}$$

5 Computational procedure: shooting approach

The shooting method [57] is employed for finding modeled equation solutions. The localized solution of equations (3.3) and (3.4), subject to (3.5) constraints, is found *via* the shooting technique. The shooting methodology is given as follows (Figure 2).

Initial order ODEs are required for this method's first step. To satisfy these criteria, conversion of (3.3)–(3.5) into first-order system yields

$$z_1 = f', \tag{5.1}$$

$$z_2 = z_1', \tag{5.2}$$

$$z_3 = z_2', \tag{5.3}$$

$$z_4 = \theta', \tag{5.4}$$

$$z_2' + \phi_1\left[\phi_2\left(fz_2 - {z_1}^2 - A\left(\frac{\chi}{2}z_2 + z_1\right)\right) + \alpha(2z_1z_2') + A\left(2z_2 + \frac{\chi}{2}z_3'\right) - {z_2}^2 - fz_3' - \frac{\phi_4}{\phi_2}M\sin^2(\Gamma)z_1\right] = 0, \tag{5.5}$$

$$z_4'\left(1 + \frac{1}{\phi_4}\mathrm{Pr}N_r\right) + \mathrm{Pr}\frac{\phi_3}{\phi_4}\left[fz_4 - z_1\theta - A\left(\theta + \frac{\chi}{2}z_4\right) + \frac{\mathrm{Ec}}{\phi_1\phi_3}z_2^2 + \frac{\phi_4}{\phi_3}M\mathrm{Ec}\sin^2(\Gamma)z_1^2\right] = 0, \tag{5.6}$$

$$f(0) = S, z_1(0) = 1 + \Lambda z_2(0), \quad z_3(0) = -B_\varsigma(1 - \theta(0)), z_1(\infty) \to 0, \quad z_2(\infty) \to 0, \theta(\infty) \to 0. \tag{5.7}$$

6 Code validation

Although this approach was tested by comparing its heat transfer rate findings to those found in earlier studies [58–61], it was shown to be valid. Comparing the levels of consistency found across the various research is summarized in Table 3. It is important to note that the findings of this study are absolutely correct.

7 Numerical results and discussions

The intention of this part is to display the encouragement of several dimensionless parameters on intricate profiles. For example, the current problem indicates the SGNF stream with inclined MHD, viscous dissipation effects, and entropy analysis. Here, we have done a comparative study on copper–methanol and iron–methanol second-grade nanoliquids. In this section, we analyzed the actions

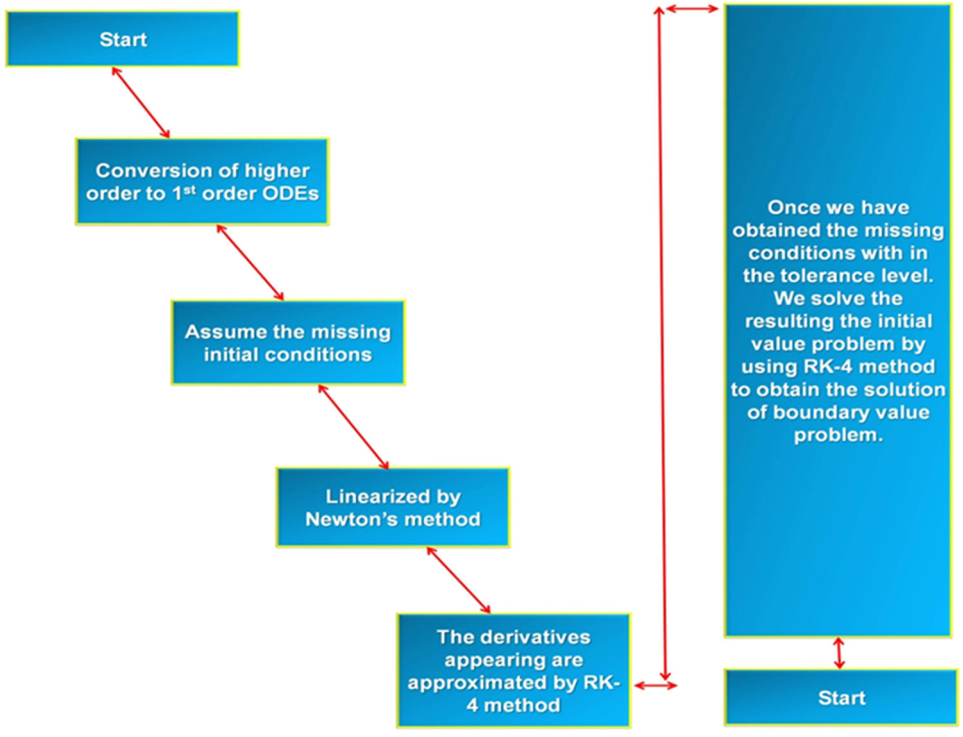

Figure 2: Shooting technique methodology.

Table 3: Comparison of $-\theta'(0)$ by variation in Prandtl number, $\phi = 0$, $A = 0$, $\Lambda = 0$, $N_r = 0$, $M = 0$, Ec = 0, $S = 0$, and $\mathrm{Bi}_{\varsigma} \to \infty$

Prandtl number (Pr)	10.0	7.0	3.0	1.0	0.72
Ishak *et al.* [58]	3.7207	3.0723	1.9237	1.0000	0.8086
Ishak *et al.* [59]	3.7006	3.0723	1.9236	1.0000	0.8086
Abolbashari *et al.* [60]	3.72067390	3.07225021	1.92368259	1.00000000	0.80863135
Das *et al.* [61]	3.72055436	3.07314679	1.92357431	1.00000000	0.80876122
Present results	3.72055429	3.07314651	1.92357420	1.00000000	0.80876181

of frequent dimensionless parameters on the respective profiles by using appropriate graphs.

Figure 3 demonstrates the sway of M on f' of both copper–methanol and iron–methanol second-grade nanoliquids. Here, the upsurge in M declines the f'. Physically, M corresponds to the Lorentz force that slows the movement of the liquid particles, resulting in the declination of f'. Furthermore, the f' of copper–methanol SGNF is strongly triggered by the magnetic field and decays faster when compared to iron–methanol SGNF. The change in f' of both nanoliquids for varied Λ is exemplified in Figure 4. Here, gain in Λ declines the f'. Furthermore, the f' for copper–methanol SGNF is strongly triggered by Λ and declines faster when compared to iron–methanol SGNF. The provocation of S on f' of both copper–methanol and iron–methanol SGNFs is demonstrated in Figure 5. The escalation in S drops the f' for both nanoliquids. Here, the f' of copper–methanol SGNF is strongly triggered by S and declines faster when compared to iron–methanol SGNF. Figure 6 displays the sway of α on f' of both copper–methanol and iron–methanol SGNFs. The gain in α progresses the f'. Moreover, the f' of iron–methanol SGNF is strongly exaggerated by α and inclines faster when compared to copper–methanol SGNF.

Figure 7 reveals the upshot of Eckert number on the thermal profile representing both iron–methanol and

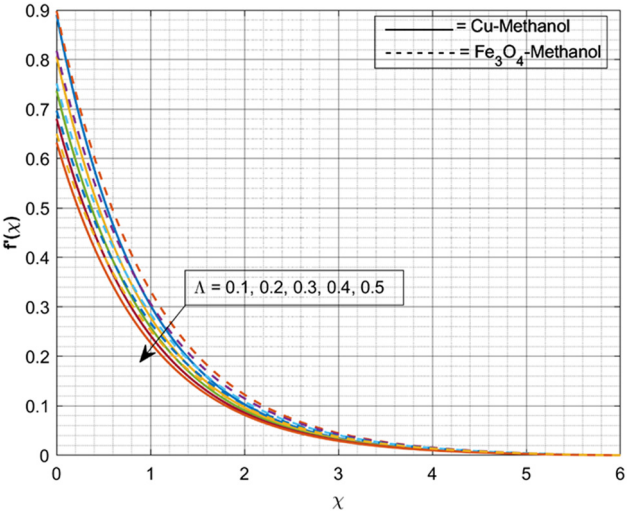

Figure 4: Sway of Λ on f'.

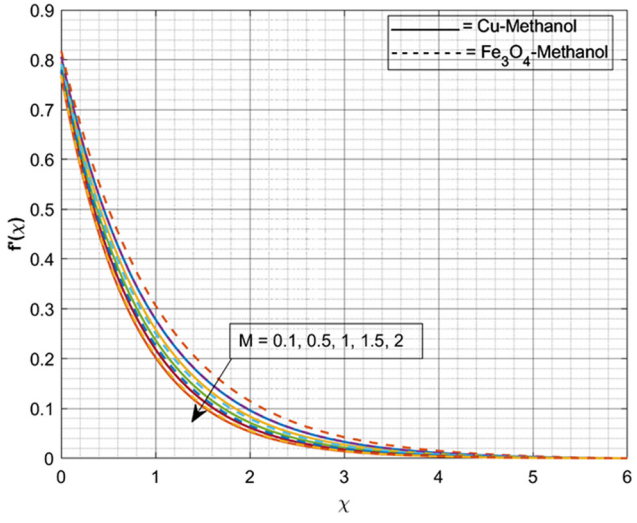

Figure 3: Sway of M on f'.

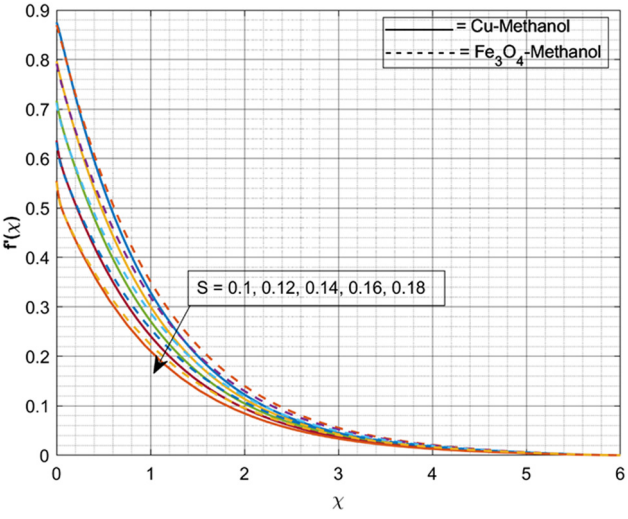

Figure 5: Sway of S on f'.

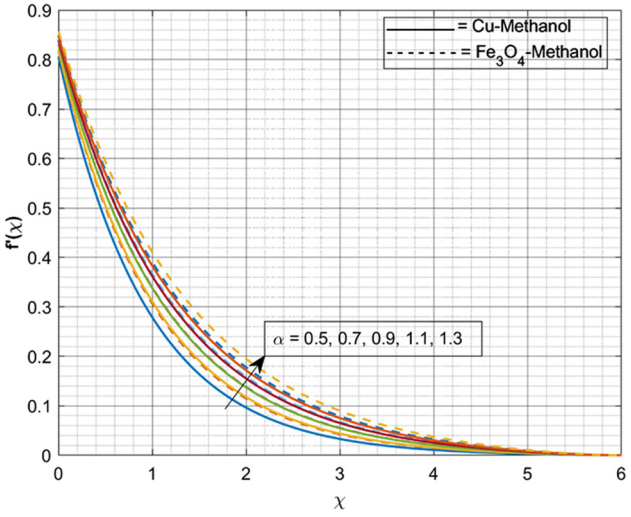

Figure 6: Sway of α on f'.

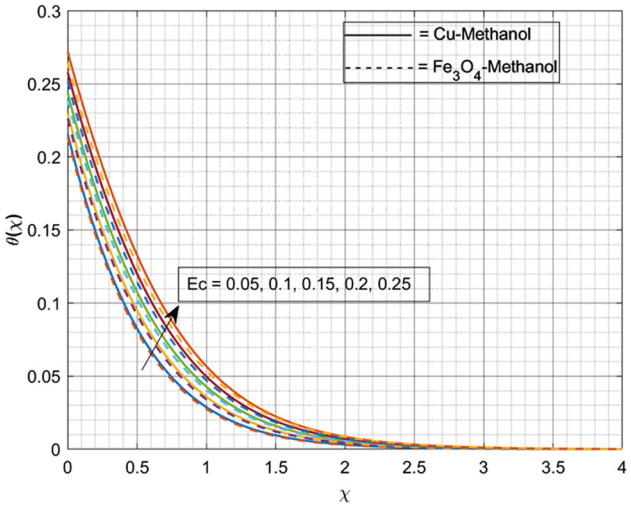

Figure 7: Sway of Ec on θ.

copper–methanol SGNFs. The rise in Ec enhances the thermal profile. It is moderately clear from the description of Ec that its higher values give rise to the strong heat effect, which raises the temperature. Here, copper–methanol SGNF shows improved heat transfer than iron–methanol SGNF for improved values of Ec. The impact of Bi_ς on thermal gradient for both copper–methanol and iron–methanol second-grade nanoliquids is depicted in Figure 8. The enhancement of Bi_ς improves the thermal profile of both nanoliquids. Physically, the boom in Bi_ς produces large heat transport *via* convection, which results in increased heat transport. Furthermore, copper–methanol SGNF shows improved heat transport than iron–methanol SGNF, for improved values of Bi_ς.

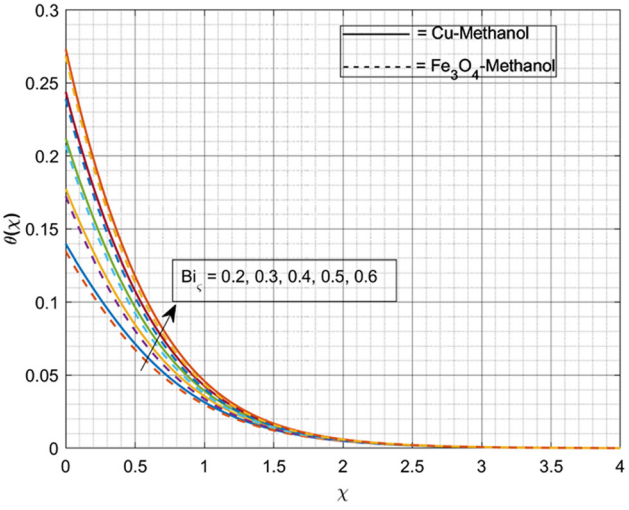

Figure 8: Sway of Bi_ς on θ.

The influence of N_r on heat transfer for both nanoliquids is typified in Figure 9. The upsurge in N_r advances the heat transference of both nanoliquids. When the N_r is inclined, internal heat is generated, resulting in increased heat transport. Furthermore, copper–methanol SGNF shows improved heat transport than iron–methanol SGNF, with improved values of N_r. The influence of M on the thermal profile of both liquids is typified in Figure 10. The increase in M enriches the thermal profile in both the fluid flows representing copper–methanol and iron–methanol second-grade nanoliquid. An increase in the magnetic parameters intensifies the magnetic field. Here, the fluid temperature gradually increases due to the thermal radiation effect, which supplies the additional heat to the flow system. Figure 11 illustrates the impact of M on the entropy

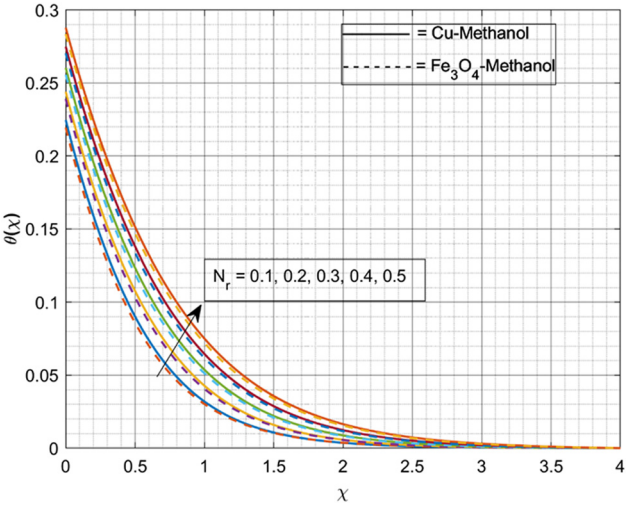

Figure 9: Sway of N_r on θ.

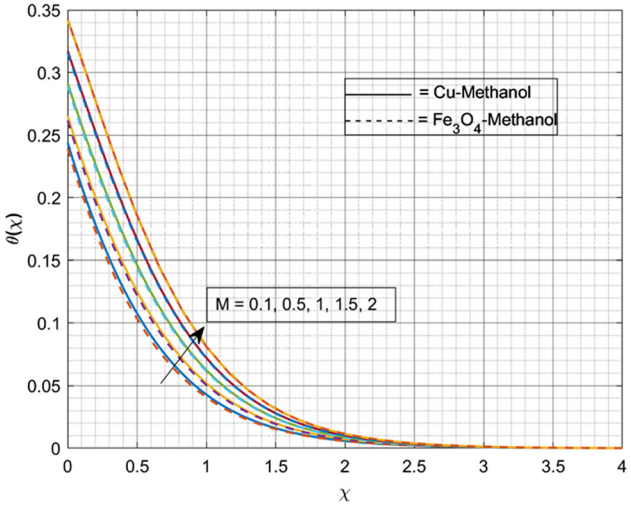

Figure 10: Sway of M on θ.

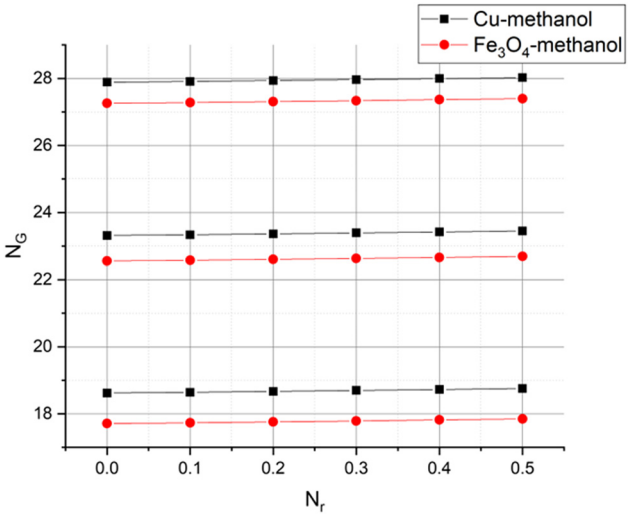

Figure 11: Sway of N_r on NG.

generation profile *versus* radiation parameter for both nanoliquids. The upsurge in magnetic parameters improves the entropy generation of both iron–methanol and copper–methanol SGNFs. Moreover, the entropy generation profile of copper–methanol SGNF is strongly affected and inclines faster when compared to iron–methanol SGNF, for improved values of both M and N_r.

The encouragement of various non-dimensional parameters on Nusselt number and skin friction for both iron–methanol and copper–methanol second-grade nanoliquids are tabulated in Tables 4 and 5. The impact of S, N_r, M, Λ, ϕ, α, Bi, γ, and A on surface drag force is displayed in Table 5.

In this case, increasing the values of S, M, ϕ, α, Bi_{ς}, γ, and A decreases the friction factor of both nanoliquids. But the conflicting trend is portrayed as boosting the values of Λ for both iron–methanol and copper–methanol second-grade nanoliquids. Table 4 displays the consequences of N_r, M, Λ, ϕ, α, Bi_{ς}, γ, and A on the rate of heat transference of both iron–methanol and copper–methanol SGNFs. It is interesting to note from the table that the escalation in N_r, α, and Bi improves the rate of heat transport in both SGNFs. But the conflicting trend is seen to boost up the values of Λ.

8 Final remarks

In this study, relative requests of the stream for the copper and iron non-Newtonian methanol-based nanofluids were accomplished over a piercing level plane surface with a non-uniform extending speed. The examination was conducted in the event of various physical

Table 4: Influence of varied dimensional parameters on Nusselt number

M	N_r	Ec	Bi_{ς}	α	A	Λ	γ	S	ϕ	$\mathrm{NuRe}_x^{-1/2}$ Cu–methanol	$\mathrm{NuRe}_x^{-1/2}$ Fe_3O_4–methanol
0.1	0.2	0.15	0.5	0.5	0.4	0.2	$\pi/2$	0.5	0.02	0.51278	0.512147
										0.510233	0.509482
0.3										0.507687	0.506817
	0.1									0.484522	0.483892
	0.15									0.498614	0.497982
		0.1								0.519784	0.518999
		0.2								0.505777	0.505421
			0.4							0.4239	0.478266
			0.6							0.596058	0.451237
				0.6						0.514054	0.513416
				0.7						0.5152	0.514431
					0.5					0.512653	0.51202
					0.6					0.512526	0.511893

Table 5: Influence of varied dimensional parameters on skin friction

M	S	Λ	ϕ	A	α	Bi_{ς}	γ	N_r	Ec	$C_f Re_x^{\frac{1}{2}}$ Cu–methanol	$C_f Re_x^{\frac{1}{2}}$ Fe_3O_4–methanol
0.1	0.5	0.2	0.02	0.4	0.5	0.5	$\pi/2$	0.2	0.15	−2.15294	−2.0902
0.2										−2.19105	−2.13351
0.3										−2.22811	−2.17525
	0.2									−1.94159	−1.8929
	0.3									−2.01037	−1.95713
		0.1								−2.49201	−2.40893
		0.3								−1.89158	−1.84274
			0.01							−2.12828	−2.09517
			0.03							−2.17136	−2.08288
				0.5						−2.18766	−2.12508
				0.6						−2.2233	−2.16011
					0.6					−2.34291	−2.27535
					0.7					−2.52543	−2.45309

impacts. The primary comments of the present review are as follows:

- The velocity of copper–methanol SGNF is sturdily triggered by the suction parameter and declines faster than iron–methanol SGNF.
- The velocity of copper–methanol SGNF is sturdily triggered by a magnetic field and drops faster than iron–methanol SGNF.
- The velocity of iron–methanol SGNF is strongly exaggerated by α and inclines faster than copper–methanol SGNF.
- Copper–methanol SGNF shows improved heat transport than iron–methanol SGNF for improved values of Bi_{ς}.
- Copper–methanol SGNGF shows improved heat transport than iron–methanol SGNF for improved values of Ec.
- The entropy generation profile of copper–methanol SGNF is strongly affected and inclines faster when compared to iron–methanol SGNF for improved values of both magnetic and thermal radiation parameters.
- Copper–methanol SGNF shows an improved rate of heat transference than iron–methanol SGNF.
- The shooting method could be applied to a variety of physical and technical challenges in the future [62–71].

Acknowledgments: The author Rangaswamy Naveen Kumar is thankful to Department of OBC and minority cell, Davangere University, Davangere, Karanataka, INDIA for financial support Fellowship 1/2021-22/6998.

Funding information: The authors state no funding involved.

Author contributions: All authors have accepted responsibility for the entire content of this manuscript and approved its submission.

Conflict of interest: The authors state no conflict of interest.

References

[1] Sahoo B. Effects of slip, viscous dissipation and Joule heating on the MHD flow and heat transfer of a second-grade fluid past a radially stretching sheet. Appl Math Mech. 2010;31(2):159–73.

[2] Imtiaz M, Kiran A, Hayat T, Alsaedi A. Joule heating and MHD effects in flow of second-grade fluid due to a rotating disk with variable thickness. Phys Scr. 2019;94(8):085203.

[3] Hayat T, Khan WA, Abbas SZ, Nadeem S, Ahmad S. Impact of induced magnetic field on second-grade nanofluid flow past a convectively heated stretching sheet. Appl Nanosci. 2020;10(8):3001–9.

[4] Kalaivanan R, Ganesh NV, Al-Mdallal QM. An investigation on Arrhenius activation energy of second grade nanofluid flow with active and passive control of nanomaterials. Case Stud Therm Eng. 2020;22:100774.

[5] Wakeel Ahmad M, McCash LB, Shah Z, Nawaz R. Cattaneo-Christov heat flux model for second grade nanofluid flow with Hall effect through entropy generation over stretchable rotating disk. Coatings. 2020;10(7):610.

[6] Shafiq A, Rasool G, Khalique CM, Aslam S. Second grade bioconvective nanofluid flow with buoyancy effect and chemical reaction. Symmetry. 2020;12(4):621.

[7] Gowda RJP, Kumar RN, Aldalbahi A, Prasannakumara BC, Gorji MR, Rahaman M. Thermophoretic particle deposition in time-dependent flow of hybrid nanofluid over rotating and

vertically upward/downward moving disk. Surf Interfaces. 2021;22:100864.
[8] Christopher AJ, Magesh N, Gowda RJP, Kumar RN, Kumar RSV. Hybrid nanofluid flow over a stretched cylinder with the impact of homogeneous–heterogeneous reactions and Cattaneo–Christov heat flux: series solution and numerical simulation. Heat Transf. 2021;50:3800–21.
[9] Jayadevamurthy PGR, Kumar Rangaswamy N, Prasannakumara BC, Nisar KS. Emphasis on unsteady dynamics of bioconvective hybrid nanofluid flow over an upward–downward moving rotating disk. Numer Methods Partial Differ Equ. 2020;num.22680.
[10] Hayat T, Shah F, Alseadi A. Cattaneo-Christov double diffusions and entropy generation in MHD second grade nanofluid flow by a Riga wall. Int Commun Heat Mass Transf. 2020;119:104824.
[11] Shashikumar NS, Gireesha BJ, Mahanthesh B, Prasannakumara BC. Brinkman-Forchheimer flow of SWCNT and MWCNT magneto-nanoliquids in a microchannel with multiple slips and Joule heating aspects'. Multidiscip Model Mater Struct. 2018;14(4):769–86.
[12] Hayat T, Shah F, Alsaedi A, Ahmad B. Entropy optimized dissipative flow of effective Prandtl number with melting heat transport and Joule heating. Int Commun Heat Mass Transf. 2020;111:104454.
[13] Radhika M, Gowda RJP, Naveenkumar R, Prasannakumara BC. Heat transfer in dusty fluid with suspended hybrid nanoparticles over a melting surface. Heat Transf. 2021;50(3):2150–67.
[14] Ijaz M, Ayub M, Malik MY, Khan H, Alderremy AA, Aly S. Entropy analysis in nonlinearly convective flow of the Sisko model in the presence of Joule heating and activation energy: the Buongiorno model. Phys Scr. 2020;95(2):025402.
[15] Reddy MG, Kumar N, Prasannakumara BC, Rudraswamy NG, Kumar KG. Magneto-hydrodynamic flow and heat transfer of a hybrid nanofluid over a rotating disk by considering Arrhenius energy. Commun Theor Phys. 2021;73:045002.
[16] Hayat T, Khan MI, Alsaedi A, Khan MI. Joule heating and viscous dissipation in flow of nanomaterial by a rotating disk. Int Commun Heat Mass Transf. 2017;89:190–7.
[17] Sithole H, Mondal H, Sibanda P. Entropy generation in a second grade magnetohydrodynamic nanofluid flow over a convectively heated stretching sheet with nonlinear thermal radiation and viscous dissipation. Results Phys. 2018;9:1077–85.
[18] Hazarika S, Ahmed S, Chamkha AJ. Investigation of nanoparticles Cu, Ag and Fe_3O_4 on thermophoresis and viscous dissipation of MHD nanofluid over a stretching sheet in a porous regime: a numerical modeling. Math Comput Simul. 2021;182:819–37.
[19] Gireesha Bj, Umeshaiah M, Prasannakumara BC, Shashikumar NS, Archana M. Impact of nonlinear thermal radiation on magnetohydrodynamic three-dimensional boundary layer flow of Jeffrey nanofluid over a nonlinearly permeable stretching sheet. Phys Stat Mech Appl. 2020;549:124051.
[20] Shit GC, Mandal S. Entropy analysis on unsteady MHD flow of Casson nanofluid over a stretching vertical plate with thermal radiation effect. Int J Appl Comput Math. 2019;6(1):2.
[21] Bejan A. A study of entropy generation in fundamental convective heat transfer. J Heat Transf. 1979;101(4):718–25.
[22] Yusuf TA, Adesanya SO, Gbadeyan JA. Entropy generation in MHD Williamson nanofluid over a convectively heated stretching plate with chemical reaction. Heat Transf. 2020;49(4):1982–99.
[23] Azam M, Mabood F, Xu T, Waly M, Tlili I. Entropy optimized radiative heat transportation in axisymmetric flow of Williamson nanofluid with activation energy. Results Phys. 2020;19:103576.
[24] Bhatti MM, Riaz A, Zhang L, Sait SM, Ellahi R. Biologically inspired thermal transport on the rheology of Williamson hydromagnetic nanofluid flow with convection: an entropy analysis. J Therm Anal Calorim. 2021;144:2187–202.
[25] Alsaadi FE, Hayat T, Khan MI, Alsaadi FE. Heat transport and entropy optimization in flow of magneto-Williamson nanomaterial with Arrhenius activation energy. Comput Methods Prog Biomed. 2020;183:105051.
[26] Hayat T, Shafiq A, Alsaedi A. MHD axisymmetric flow of third grade fluid between stretching sheets with heat transfer. Comput Fluids. 2015;86:103–8.
[27] Hayat T, Shafiq A, Alsaedi A, Shahzad SA. Unsteady MHD flow over exponentially stretching sheet with slip conditions. Appl Math Mech. 2016;37(2):193–208.
[28] Shafiq A, Hammouch Z, Sindhu TN. MHD flow of tangent hyperbolic nanofluid with Newtonian heating. Int J Mech Sci. 2017;133:759–66.
[29] Shafiq A, Sindhu TN. Statistical study of hydromagnetic boundary layer flow of Williamson fluid regarding a radiative surface. Results Phys. 2017;7:3059–67.
[30] Shafiq A, Rasool G, Khalique CM. Significance of thermal slip and convective boundary conditions in three dimensional rotating Darcy-Forchheimer nanofluid flow. Symmetry. 2020;12(5):741.
[31] Shafiq A, Sindhu TN, Khalique CM. Numerical investigation and sensitivity analysis on bioconvective tangent hyperbolic nanofluid flow towards stretching surface by response surface methodology. Alex Eng J. 2020;59(6):4533–48.
[32] Rahman A, Lone SA, Sindhu TN, Kamal M. Statistical inference for Burr Type X distribution using geometric process in accelerated life testing design for time censored data. Pak J Stat Oper. 2020;16(3):577–86.
[33] Shafiq A, Lone SA, Sindhu TN, Khatib YE, Al-Mdallal QM, Muhammad T. A new modified Kies Fréchet distribution: Applications of mortality rate of Covid-19. Results Phys. 2021;28:104638.
[34] Shafiq A, Lone SA, Sindhu TN, Al-Mdallal QM, Rasool G. Statistical modeling for bioconvective tangent hyperbolic nanofluid towards stretching surface with zero mass flux condition. Sci Rep. 2021;11(1):1–11.
[35] Shafiq A, Çolak AB, Sindhu TN, Al-Mdallal QM, Abdeljawad T. Estimation of unsteady hydromagnetic Williamson fluid flow in a radiative surface through numerical and artificial neural network modeling. Sci Rep. 2021;11(1):1–21.
[36] Shafiq A, Sindhu TN, Al-Mdallal QM. A sensitivity study on carbon nanotubes significance in Darcy-Forchheimer flow towards a rotating disk by response surface methodology. Sci Rep. 2021;11(1):1–26.
[37] Sindhu TN, Shafiq A, Al-Mdallal QM. Exponentiated transformation of Gumbel Type-II distribution for modeling COVID-19 data. , Alex Eng J. 2021;60(1):671–89.

[38] Sindhu TN, Atangana A. Reliability analysis incorporating exponentiated inverse Weibull distribution and inverse power law. Qual Reliab Eng Int. 2021;37:2399–422.
[39] Shafiq A, Çolak AB, Sindhu TN. Designing artificial neural network of nanoparticle diameter and solid-fluid interfacial layer on single-walled carbon nanotubes/ethylene glycol nanofluid flow on thin slendering needles. Int J Numer. 2021;93(12):3384–404.
[40] Shafiq A, Çolak AB, Sindhu TN, Muhammad T. Optimization of Darcy-Forchheimer squeezing flow in nonlinear stratified fluid under convective conditions with artificial neural network. Heat Transf Res. 2022;53(3):67–89.
[41] Shah Z, Alzahrani EO, Dawar A, Alghamdi W, Ullah MZ. Entropy generation in MHD second-grade nanofluid thin film flow containing CNTs with Cattaneo-Christov heat flux model past an unsteady stretching sheet. Appl Sci. 2020;10(4):2720.
[42] Reddy NB, Poornima T, Sreenivasulu P. Influence of variable thermal conductivity on MHD boundary layer slip flow of ethylene-glycol based Cu nanofluids over a stretching sheet with convective boundary condition. J Eng Math. 2014;1(10):905158.
[43] Jamshed W, Aziz A. Entropy analysis of TiO_2-Cu/EG Casson hybrid nanofluid via Cattaneo-Christov heat flux model. Appl Nanosci. 2018;08:1–14.
[44] Jamshed W. Numerical investigation of MHD impact on Maxwell nanofluid. Int Commun Heat Mass Transf. 2020;120:104973.
[45] Jamshed W, Nisar KS. Computational single phase comparative study of Williamson nanofluid in parabolic trough solar collector via Keller box method. Int J Energy Res. 2021;45:10696–718.
[46] Jamshed W, Akgül EK, Nisar KS. Keller box study for inclined magnetically driven Casson nanofluid over a stretching sheet: single phase model. Phys Scr. 2021;96:065201.
[47] Jamshed W, Aziz A. A comparative entropy based analysis of Cu and Fe_3O_4/methanol Powell-Eyring nanofluid in solar thermal collectors subjected to thermal radiation variable thermal conductivity and impact of different nanoparticles shape. Results Phys. 2018;9:195–205.
[48] Jamshed W, Devi S SU, Safdar R, Redouane F, Nisar KS, Eid MR. Comprehensive analysis on copper-iron (II, III)/oxide-engine oil Casson nanofluid flowing and thermal features in parabolic trough solar collector. J Taibah Univ Sci. 2021;15(1):619–36.
[49] Jamshed W, Eid MR, Nisar KS, Mohd Nasir NAA, Edacherian A, Saleel CA, et al. A numerical frame work of magnetically driven Powell-Eyring nanofluid using single phase model. Sci Rep. 2021;11:16500.
[50] Brewster MQ. Thermal radiative transfer and properties. Hoboken, New Jersey, U.S.: John Wiley and Sons; 1992.
[51] Jamshed W, Kouz WA, Mohd Nasir NAA. Computational single phase comparative study of Inclined MHD in Powell-Eyring nanofluid. Heat Transf – Asian Res. 2021;50(4):3879–912.
[52] Hussain SM, Jamshed W. A comparative entropy based analysis of tangent hyperbolic hybrid nanofluid flow: Implementing finite difference method. Int Commun Heat Mass Transf. 2021;129:105671.
[53] Jamshed W. Thermal augmentation in solar aircraft using tangent hyperbolic hybrid nanofluid: A solar energy application. Energy Env. 2022;33(6):1090–133.
[54] Jamshed W, Mishra SR, Pattnaik PK, Nisar KS, Devi SSU, Prakash M, et al. Features of entropy optimization on viscous second grade nanofluid streamed with thermal radiation: A Tiwari and Das model. Case Stud Therm Eng. 2021;27:101291.
[55] Hussain SM, Jamshed W, Safdar R, Shahzad F, Mohd Nasir NA, Ullah I. Chemical reaction and thermal characteristics of Maxwell nanofluid flow-through solar collector as a potential solar energy cooling application: A modified Buongiorno's model. Energy Env. 2021;33:1–24.
[56] Jamshed W, Nisar KS, Ibrahim RW, Shahzad F, Eid MR. Thermal expansion optimization in solar aircraft using tangent hyperbolic hybrid nanofluid: a solar thermal application. J Mater Res Technol. 2021;14:985–1006.
[57] Na TY. Computational methods in engineering boundary value problems. Vol. 145. Cambridge, Massachusetts, United States: Academic Press; 1980.
[58] Ishak A, Nazar R, Pop I. Mixed convection on the stagnation point flow towards a vertical, continuously stretching sheet. ASME, J Heat Transf. 2007;129:1090.
[59] Ishak A, Nazar R, Pop I. Boundary layer flow and heat transfer over an unsteady stretching vertical surface. Meccanica. 2009;44:375–5.
[60] Abolbashari MH, Freidoonimehr N, Nazari F, Rashidi MM. Entropy analysis for an unsteady MHD flow past a stretching permeable surface in nano-fluid. Powder Technol. 2014;267:267.
[61] Das S, Chakraborty S, Jana RN, Makinde OD. Entropy analysis of unsteady magneto-nanofluid flow past accelerating stretching sheet with convective boundary condition. Appl Math Mech. 2015;36(2):1610–75.
[62] Hussain SM, Goud BS, Madheshwaran P, Jamshed W, Pasha AA, Safdar R, et al. Effectiveness of nonuniform heat generation (Sink) and thermal characterization of a carreau fluid flowing across a nonlinear elongating cylinder: a numerical study. ACS Omega. 2022;7:25309–20.
[63] Pasha AA, Islam N, Jamshed W, Alam MI, Jameel AGA, Juhany KA, et al. Statistical analysis of viscous hybridized nanofluid flowing via Galerkin finite element technique. Int Commun Heat Mass Transf. 2022;137:106244.
[64] Hussain SM, Jamshed W, Pasha AA, Adil M, Akram M. Galerkin finite element solution for electromagnetic radiative impact on viscid Williamson two-phase nanofluid flow via extendable surface. Int Commun Heat Mass Transf. 2022;137:106243.
[65] Shahzad F, Jamshed W, Safdar R, Mohd Nasir NAA, Eid MR, Alanazi MM, et al. Thermal valuation and entropy inspection of second-grade nanoscale fluid flow over a stretching surface by applying Koo–Kleinstreuer–Li relation. Nanotechnol Rev. 2022;11:2061–77.
[66] Jamshed W, Eid MR, Safdar R, Pasha AA, Mohamed Isa SSP, Adil M, et al. Solar energy optimization in solar-HVAC using Sutterby hybrid nanofluid with Smoluchowski temperature conditions: a solar thermal application. Sci Rep. 2022;12:11484.
[67] Akgül EK, Akgül A, Jamshed W, Rehman Z, Nisar KS, Alqahtani MS, et al. Analysis of respiratory mechanics models with different kernels. Open Phys. 2022;20:609–15.
[68] Jamshed W, Safdar R, Rehman Z, Lashin MMA, Ehab M, Moussa M, et al. Computational technique of thermal comparative examination of Cu and Au nanoparticles suspended in sodium alginate as Sutterby nanofluid via extending PTSC surface. J Appl Biomater & Funct Mater. 2022;1–20.

[69] Akram M, Jamshed W, Goud BS, Pasha AA, Sajid T, Rahman MM, et al. Irregular heat source impact on Carreau nanofluid flowing via exponential expanding cylinder: A thermal case study. Case Stud Therm Eng. 2022;36:102190.
[70] Sajid T, Jamshed W, Safdar R, Hussain SM, Shahzad F, Bilal M, et al. Features and aspects of radioactive flow and slippage velocity on rotating two-phase Prandtl nanofluid with zero mass fluxing and convective constraints. Int Commun Heat Mass Transf. 2022;135:106074.
[71] Ali K, Ahmad S, Baluch O, Jamshed W, Eid MR, Pasha AA. Numerical study of magnetic field interaction with fully developed flow in a vertical duct. Alex Eng J. 2022;61:11351–63.